Interface state recombination in organic solar cells

R. A. Street* and M. Schoendorf
Palo Alto Research Center, Palo Alto, California 94304, USA

A. Roy and J. H. Lee
Center for Polymers and Organic Solids, University of California at Santa Barbara, Santa Barbara, California 93106, USA

(Received 7 October 2009; revised manuscript received 12 April 2010; published 7 May 2010)

Recombination in bulk heterojunction organic solar cells based on polycarbazole/fullerene blends are studied through measurements of the solar-cell response. Different recombination mechanisms are analyzed, including recombination of the charge-transfer exciton, Auger recombination, and recombination at interfacial localized states. The measured recombination kinetics, the temperature dependence of the current-voltage characteristics, the dark forward bias diode current, and modeling studies, all indicate that the dominant recombination is through interface states between the polymer and fullerene domains, with an estimated density of order 10^{11} cm^{-2}. Modeling studies indicate that a tenfold reduction in the interface state density could potentially double the solar-cell efficiency.

DOI: 10.1103/PhysRevB.81.205307 PACS number(s): 73.50.Gr, 71.20.Rv

I. INTRODUCTION

Organic solar cells have reached a conversion efficiency of about 6% and continue to improve.[1] The key development was the creation of the bulk heterojunction (BHJ) device, formed from a blend of a polymer and a fullerene, which phase separates into a nanoscale morphology.[2] Several different polymers have been shown to give effective solar cells of this type.[3] The BHJ cell is an example of a vertically structured cell and this design promises to be broadly important for photovoltaics.[4] Vertical cells have the advantage that the optical absorption and the charge generation or collection can be independently optimized. It is therefore important to understand the recombination mechanisms, both to improve the specific BHJ cells and to understand the general properties of vertical cells. Numerous papers have been published discussing the operation of the BHJ organic solar cell,[5,6] including several models of the solar-cell response,[7–11] but there remains considerable disagreement over the details of the recombination and charge collection mechanisms.

The basic processes in the operation of the BHJ polymer/PCBM (phenyl C_{60}–butyric acid methyl ester) solar cell are well understood. Incident light is absorbed in the polymer and the PCBM domains and creates tightly bound excitons. The excitons migrate rapidly to the interface and split into an electron in the PCBM and a hole in the polymer, which are collected by the device contacts. The collection of charge is enhanced and the recombination inhibited by the energy barriers resulting from the electronic structure of the polymer/PCBM heterojunction.

The solar-cell current, J_G, under illumination, G, and at voltage, V, can be expressed as a combination of the dark diode current and the photocurrent,

$$J_G(V) = J_{DARK}(V) - eP_C(V)G_{PH}, \tag{1}$$

where G_{PH} is the absorbed illumination intensity that contributes to charge generation and J_{DARK} is the dark diode current.[12] By the definition of Eq. (1), $eP_C(V)G_{PH}$ is the photocurrent, so that $P_C(V)$ is the photocurrent normalized to the illumination G_{PH}, and is also the probability of charge collection as a function of bias voltage. The separation of the dark current and the photocurrent according to Eq. (1) is only accurate if the voltage drop due to series resistance in the cell is negligible, and we show below that this condition applies to these measurements.

An ideal cell with no recombination has $P_C(V)=1$ but $P_C(V)$ is reduced due to recombination in a real device. The recombination primarily influences the cell fill factor. Under short circuit conditions the internal electric field is large enough to ensure that most of the charge is reaches the contacts. Recombination tends to increase in forward bias because the internal field decreases. The resulting loss of fill factor is a significant limitation on the cell efficiency and is therefore important to understand in detail

The aim of the paper is to understand the recombination mechanisms that determine $P_C(V)$. At sufficiently large reverse bias, $P_C=1$ and the reverse saturation photocurrent, $J_{GSAT}=eG_{PH}$. According to this definition G_{PH} is the incident flux that is absorbed in the solar cell, minus any recombination mechanisms that are not dependent on the bias, examples of which are recombination of the exciton before it reaches the interface and excitons that result in uncollectible charge because of the film morphology. The paper considers the different recombination mechanisms that might influence $P_C(V)$ and compares the experimental evidence for each mechanism. We conclude that the combined evidence of different experiments favors the mechanism of carrier recombination at interface states near the heterojunction, instead of the primary alternative of geminate recombination at the charge-transfer exciton (CTE).

Section II describes the samples, the measurement techniques, and the experimental results, including room-temperature and low-temperature measurements of the cell characteristics and the spectral response. Section III analyzes the different possible recombination mechanisms and compares their ability to account for the current-voltage characteristics. Section IV discusses further evidence for the conclusion that recombination is dominated by interface states, which is obtained from an analysis of the forward diode

characteristics and the temperature dependence of the current-voltage data. A simple model for the open circuit voltage is also reported.

II. MEASUREMENTS AND RESULTS

Samples were fabricated at UC Santa Barbara, as described in Ref. 4. The blend comprises an alternating poly(2,7-carbazole), PCDTBT,[13] and the fullerene, [6-6]-phenyl C_{70}-butyric acid methyl ester ($PC_{70}BM$).[14,15] Briefly, solar cells were fabricated on an indium tin oxide (ITO)-coated glass substrate with the following structure; ITO-coated glass substrate/poly(3,4-ethylenedioxythiophene); poly (styrenesylfonate) (PEDOT:PSS)/PCDTBT:$PC_{70}BM$/TiO_x/Al. PEDOT:PSS (Baytron PH) was spin cast from aqueous solution to form a film of 40 nm thickness. The substrate was dried for 10 min at 140 °C in air and then transferred into a nitrogen-filled glove box to spin cast the charge separation layer. A solution containing a mixture of PCDTBT:$PC_{70}BM$ (1:4) in dichlorobenzene was then spin cast on top of the PEDOT/PSS layer. The film was dried for 60 min at 70 °C in a nitrogen-filled glove box. The TiO_x precursor solution diluted by 1:200 in methanol was spin cast in air on top of the PCDTBT:$PC_{70}BM$ layer (5000 rpm for 40 s). The sample was heated at 80 °C for 10 min in air. Then, an aluminum (Al, 100 nm) electrode was deposited by thermal evaporation in a vacuum of about 5×10^{-7} Torr. The efficiency of the specific devices were measured under a solar simulator at Santa Barbara, with typical results as follows; open circuit voltage, 0.84 V; short circuit current, 10.5 mA/cm^2; fill factor 0.59; efficiency 5.2%. The devices have an area of 0.18 cm^2. Six samples were measured and sample-to-sample variations were small.

For the data described in this paper, the photocurrent at high light intensity was measured using a white incandescent light source which evenly illuminated the solar cell. Measurements at low light intensity and the spectral response of the solar-cell samples were measured using a monochromator and lock-in amplifier. The light source was a quartz tungsten halogen lamp. A quarter meter grating monochromator produced light in the range 350–1200 nm. A chopper modulated the light usually at 230 Hz and this modulated beam was focused by a lens to illuminate the device. Cutoff filters were used to remove higher-order wavelengths and other scattered light from the monochromator. The sample had an adjustable bias voltage and a 9 kΩ series resistor to provide the voltage input to the lock-in amplifier. In a few situations the current was large enough that a correction was needed for the voltage drop across the resistor. For both types of measurement, the light intensity was measured with a calibrated power meter. Low-temperature measurements were made with the sample attached to a cold finger cryostat, cooled with liquid nitrogen. The device was held while cool for long enough to allow the sample temperature to equilibrate and then measured while being warmed up slowly.

Figure 1 shows room-temperature measurements of the dark and illuminated solar-cell current under white light at roughly 10% of solar illumination intensity. The data with the dark current subtracted therefore represents $eP_C(V)G_{PH}$ in Eq. (1). It is evident that the current tends to an asymptotic value at large reverse bias, where $P_C(V)=1$ and $P_C(V)$ drops to zero near 0.85 V. The subtraction of the dark current only makes a significant difference near the open circuit voltage V_{OC} but at low light intensity the dark current is larger than the photocurrent over a wide range. The dashed line in Fig. 1 is the dark current minus J_{GSAT} and is therefore an estimate of the response that the cell would have in the absence of any recombination. The recombination therefore mainly has the effect of reducing the cell fill factor.

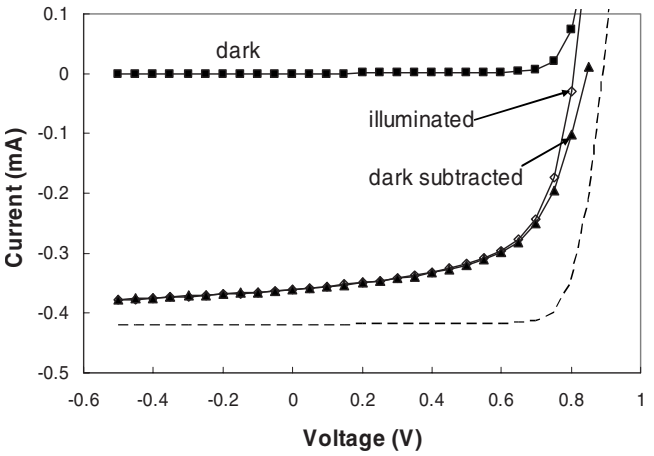

FIG. 1. Measurement of the dark, illuminated, and subtracted BHJ organic solar-cell current, for white light illumination. The dashed line is the dark current minus the reverse saturation current.

Figure 2 shows a set of normalized photoconductivity characteristics, $P_C(V)$, under white light illumination covering a 30-fold range of illumination intensities. The data is obtained from the measured photocurrent with the dark current subtracted and normalized to an extrapolated reverse bias value which represents G_{PH}. The $P_C(V)$ characteristics are virtually identical at the different illumination intensities and the reverse bias saturation current is found to be propor-

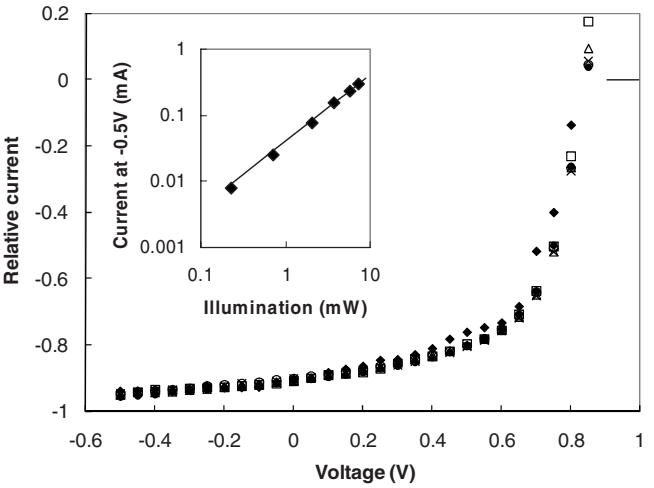

FIG. 2. Solar-cell $P_C(V)$ characteristics with white light illumination with a range of light intensities. The inset shows the reverse saturation current versus illumination intensity and the solid line has slope=1.

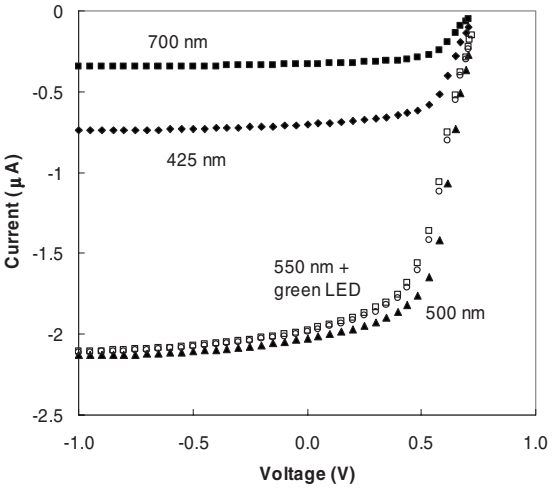

FIG. 3. Solar-cell response at low illumination levels, measured with a lock-in amplifier. Illumination is with chopped monochromatic light at the wavelengths indicated and with bias light from a green LED (wavelength 530 nm) at two different intensities (open data points).

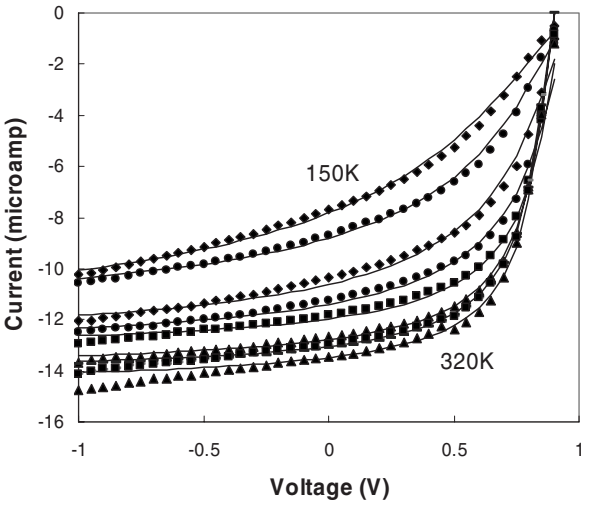

FIG. 4. Solar-cell measurement of $P_C(V)$ as a function of temperature. The solid lines are fits to the model described in Sec. III E.

tional to the light intensity. The photocurrent drops to zero and changes sign at ~0.85 eV. This voltage, which we define as V_S is always slightly larger than the cell open circuit voltage V_{OC}. The region of positive photocurrent at $V > V_S$ was not studied in detail since the dark current becomes much larger than the photocurrent. We do not observe the shifted S-shaped response reported by Ooi *et al.*,[16] which appears to be due to the specific properties of the contacts.

Figure 3 shows similar data at much lower illumination levels and for a different device. The data are measured with chopped monochromatic illumination using a lock-in amplifier with and without a dc bias illumination with a green light-emitting diode (LED). The lock-in technique automatically subtracts the dark diode current which is now larger than the photocurrent except near $V=0$. The shape of the data is similar to the higher intensity data in Fig. 1, and the shows that the form of $P_C(V)$ hardly changes over a wide range of illumination intensities and illumination conditions, and that V_S is reasonably independent of illumination intensity. A significant conclusion from the linear results in Figs. 2 and 3 is that the recombination processes described by $P_C(V)$ have monomolecular recombination kinetics over several orders of magnitude in current. Bimolecular kinetics would result in an increasing rate of recombination as the intensity increases and a corresponding change in the shape of $P_C(V)$.

Figure 4 shows the temperature dependence of $P_C(V)$ from 150 to 320 K, under white light illumination of intensity about 2 $\mathrm{mW/cm^2}$. The curve of $P_C(V)$ becomes steadily flatter at lower temperatures and the voltage V_S, when $J_{PH}(V)=0$, increases slightly. The lines in Fig. 4 are fits to a model discussed in Sec. III E. A second sample was measured and gave similar results for the shape of $P_C(V)$ but the current decreased by as much as 1000× at low temperature. We have no obvious explanation for the difference but presumably some mechanism is shutting off parts of the cell.

Figure 5 shows the spectral response quantum efficiency of the room-temperature solar-cell current under short circuit conditions, plotted as the ratio of collected electrons to incident photons (IPCE). The region above 2 eV agrees well with other data on the same type of cell and has a maximum IPCE of about 60%.[3] The measurement focuses on the response at low energy below the absorption edge of the device component materials, which is at about 1.9 eV. There is weak but significant photocurrent extending down to photon energies of 1 eV. The IPCE spectrum shows no significant change with bias light illumination, which further confirms that the photocurrent is linear in the light intensity over a wide range.

Figure 6 shows the room-temperature dark forward bias characteristics of one of the cells and its form is typical of the BHJ cells. The common diode equation for the current, J, including a series resistance R_S and a parallel shunt resistance R_P, is

$$J_{DARK}(V) = J_0\left[\exp\left(\frac{e(V-JR_S)}{nkT}\right)-1\right]+\frac{V-JR_S}{R_P}. \quad (2)$$

From the fit of this expression to the data in Fig. 6, the extrapolated reverse saturation current, J_0 is $\sim 4\times 10^{-12}$ $\mathrm{A/cm^2}$ and the ideality factor $n \sim 1.65$. The ex-

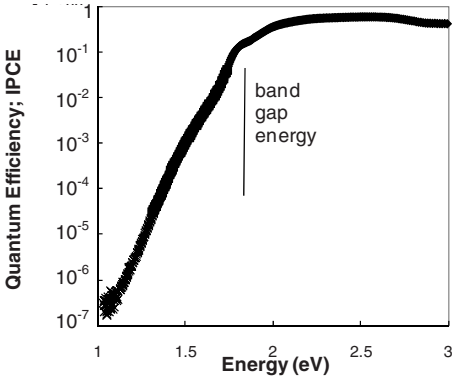

FIG. 5. Spectral response of the solar-cell IPCE, measured using lock-in techniques with a series of cutoff filters to eliminate light leakage from the spectrometer.

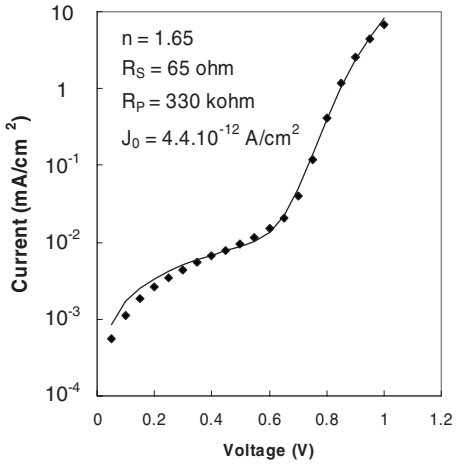

FIG. 6. Measurement of a solar-cell dark forward bias characteristic. The solid line is a fit to Eq. (2) with the parameters shown.

ponential diode region is only observed over a limited range due to the presence of an Ohmic shunt resistance which dominates at low current, and a series resistance at higher current, so the ideality factor has an uncertainty of ~0.05, and J_0 has uncertainty of at least an order of magnitude. The series resistance is only significant above about 0.9 V and so does not influence the shape of $P_C(V)$, as given by Eq. (1) and shown in Fig. 2. Other BHJ solar cells [i.e. poly(3–hexyl thiophene)/PCBM] show more of the diode region and have ideality factor ~1.8.[11]

III. ANALYSIS OF RECOMBINATION MECHANISMS

The shape of $P_C(V)$ for the solar cell reflects recombination processes that depend on the applied bias and hence on the internal electric field and/or the carrier concentrations. Most studies have focused on the electric field ionization of the electron-hole pair after the exciton is split at the interface as the primary recombination mechanism.[17,18] However there are alternative possibilities to consider at different stages of the charge collection, as follows.

(A) *Recombination of the exciton before it reaches the interface.* An exciton generated in the polymer could recombine with a hole by an Auger process and similarly an exciton in the PCBM can recombine with an electron. These are bimolecular recombination mechanisms since the rate depends on the product of the exciton and hole concentrations, both of which are proportional to the optical generation rate.

(B) *Field ionization of the geminate CTE.* When the exciton reaches the interface, it splits into an electron in the PCBM and a hole in the polymer, which are presumed to form a bound geminate electron-hole pair (the CTE), as described in more detail later. The internal electric field in the cell reduces the barrier for electron-hole separation and so the charge collection increases with reverse bias. This is a monomolecular recombination mechanism and is the mechanism most often applied to explain the photocurrent response.

(C) *Nongeminate recombination of the charge-transfer exciton.* If the electron and hole separate at the interface, there is a probability that a free electron and a free hole will meet at the interface and recombine as a charge-transfer exciton, with each carrier on a different side of the interface. This is a bimolecular mechanism. The difference in recombination kinetics arises because the geminate pair originates from one initial exciton and the nongeminate pair originates from two different excitons.

(D) *Recombination through interface states in the middle of the interface gap.* This mechanism supposes that there are defect or impurity states in the interface band gap and physically at or near the interface that can trap electrons and holes and hence allow recombination. The states might be in a narrow energy band or broadly distributed across the gap. The recombination has monomolecular kinetics, provided that the density of states is larger than the density of carriers.

(E) *Reverse diffusive recombination at the contacts.* Free carriers can diffuse against the internal field and therefore could recombine at the metal contacts. This mechanism is known to be significant when the carriers are created very close to the contact since the diffusion length exceeds the drift length at short enough times. However, in the organic solar cell, the carriers are created near the internal heterojunction, and diffusive recombination at this interface is included in mechanisms B and C. For a carrier created in the middle of the cell, back diffusion to the contact against the built-in voltage is only probable if the built in voltage is a few times kT, and therefore could be significant within about 0.1 V from V_S (i.e. above about 0.7 V), but will not significantly affect the shape of $P_C(V)$ over the wider voltage range. The voltage range over which the back diffusion has an effect scales with kT,[19] and so this mechanism predicts a steeper shape for $P_C(V)$ at low temperature. Figure 4 shows exactly the opposite behavior, and therefore we do not consider this mechanism further. These five mechanisms are illustrated in Fig. 7.

A. Numerical estimates of cell parameters

It helps to start with some estimates of carrier concentrations and other quantities that are used in the analysis. The cell thickness, d, is about 100 nm and we assume that the internal domains have dimensions of 20–30 nm. Even though the domain structure is disordered,[20] and it is known that the composition changes across the cell, for simplicity we model the domain as a cylinder of radius 15 nm. The volume of such a domain is therefore $\sim 10^{-16}$ cm^3, and hence the density is $\sim 10^{16}$ cm^{-3}. The disordered domains in the real cell will modify the quantitative results discussed below but we believe they will not affect the qualitative arguments.

At the normal solar illumination intensity (100 mW/cm^2) the reverse saturation photocurrent is ~10 mA/cm^2, which directly provides the value of G_{PH}. The effective photon flux on the surface is $\sim 6 \times 10^{16}$ ph/cm^2, which corresponds to an assumed uniform bulk illumination of G_{PH} $\sim 6 \times 10^{21}$ ph/cm^3 for a cell thickness of 100 nm.

The photoexcited hole concentration is $N_H = G_{PH} \tau_H$, where τ_H is the hole lifetime in the polymer and a similar expression applies to electrons. The hole density depends on the voltage and is a maximum at V_S because the collection

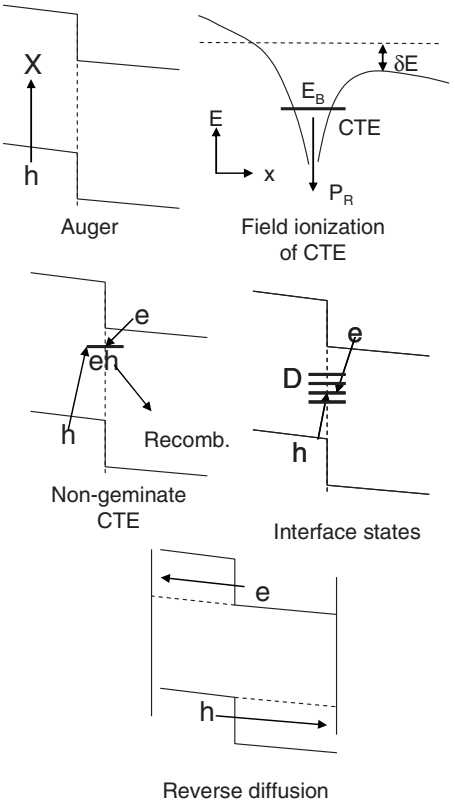

FIG. 7. Illustration of four possible bias-dependent recombination mechanisms that are described in the text.

field drops to zero, and N_H decreases as the collection voltage, $V_C = V_S - V$, is increased. The hole collection time is $d^2/\mu V_C$, where d is the effective collection length and μ is the mobility. Since, from the shape of $P_C(V)$, collection is evidently quite large at a voltage $V_C = 0.25$ V, we estimate a room-temperature hole lifetime of 10^{-7} s, assuming a mobility of 10^{-3} $\mathrm{cm}^2/\mathrm{V\,s}$ (a typical measured value) and an average collection length of 50 nm (half the thickness of the cell since holes are generated throughout the cell),

An alternative estimate of the lifetime at V_S, uses a measurement result described later that $\mu\tau = 3\times10^{-10}$ cm^2/V, from which $\tau = 3\times10^{-7}$ s^{-1}, using the same values of mobility, giving a similar estimate as above. As far as we know, the mobility of PCBM is similar to that of the polymer, so that the same estimated values for the electron lifetime apply.

Combining the generation rate and the carrier lifetime gives the carrier concentration, $N_H \sim 2\times10^{15}$ cm^{-3} at V_S, and decreasing as the collection voltage and the corresponding collection field increase. Given the estimated size of each material domain in the phase separated blend, this density corresponds to 0.2 holes /domain at V_S and 1 sun illumination. The hole concentration decreases as the collection voltage increases, and since the mobility is thermally activated, the hole concentration increases at low temperature.

The density of states at the valence-band edge, N_V is estimated to be $\sim10^{22}$ $\mathrm{cm}^{-3}\,\mathrm{eV}^{-1}$,[21] from typical polymer properties, and absent other information we assume the same value for the conduction band of PCBM. Calculations for P3HT give 2×10^{14} $\mathrm{cm}^{-2}\,\mathrm{eV}^{-1}$ for the interface density of states at the band edge,[21] and the concentration of interface atoms is similar, at $\sim10^{14}$ cm^{-2}.

The quasi-Fermi energy (QFE) is the position of the Fermi energy that leads to an equilibrium hole concentration of N_H, in units of per cubic centimeter. The QFE is found from

$$N_H = N_V kT \exp(-E_{\mathrm{QF}}/kT),$$

$$E_{\mathrm{QF}} = kT \ln(kTN_V/N_H) \approx 12kT = 0.3 \text{ eV} \qquad (3)$$

The hole concentration estimate of 2×10^{15} cm^{-3} corresponds to a sheet charge density, Q, of $\sim3\times10^{-9}$ $\mathrm{C/cm}^2$. The capacitance of the cell per unit area, $C = \varepsilon\varepsilon_0/d$, is about 3×10^{-8} $\mathrm{F/cm}^2$, assuming a dielectric constant, ε_0, of 3, and hence the ratio Q/C is 0.1 V. The small voltage implies that space charge effects are minimal and that it is reasonable to neglect charge-induced distortions of the internal field of the solar cell. However, devices with a substantially lower mobility might have significant space charge effects. All of the models discussed below assume a uniform electric field in the device.

The next part of the paper analyzes the alternative recombination mechanisms in more detail.

B. Auger recombination of the exciton

The initial exciton that is optically excited in the polymer has a reported lifetime of $\sim10-100$ fs.[22] The Auger mechanism would therefore have to be very fast to compete with this rate and hence is highly unlikely. Supporting evidence against this mechanism is the steady state estimate of not more than 0.2 holes in each domain of the blend, so there are usually no holes for the exciton to recombine with. In addition, this is a bimolecular recombination mechanism and the data indicate that the dominant mechanism is monomolecular.

C. Field ionization of the CTE

Most previous studies have attributed the recombination to field ionization of the geminate CTE, but many recognize that it is difficult to make the model work and have proposed a number of explanations, based on specific structures or internal fields at the interface.[5,23] The reason why the CTE exciton does not recombine with high probability before the electron and hole separate is that the CTE must be sufficiently shallow to allow a reasonably probability of escape, as discussed elsewhere.[24] Field ionization of the CTE is observed in photoluminescence in BHJ cells with a different polymer and the binding energy is deduced to be 0.2–0.25 eV.[17]

The exciton energy, E_B, at which there is a high probability for zero-field ionization of the CTE is estimated as follows (see Fig. 8). The rate of ionization is $\omega_0 \exp(-E_B/kT)$, where ω_0 is a rate prefactor and the rate of recombination is K_R. Hence ionization occurs when

$$K_R \ll \omega_0 \exp(-E_B/kT), \quad E_B < kT \ln(\omega_0/K_R). \qquad (4)$$

We expect that $\omega_0/K_R \sim 10^4$ (typical values are $\omega_0 \sim 10^{12}-10^{13}$ s^{-1} and $K_R \sim 10^8-10^9$ s^{-1}) so that $E_B < 10kT$ or 0.25 eV at room temperature. An exciton in a polymer has

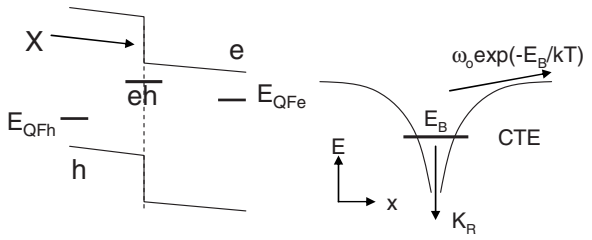

FIG. 8. Illustration of the charge-transfer exciton ionization and recombination mechanism as described in the text.

a binding energy of ~0.5 eV, but the CTE must have a smaller binding energy because the electron and hole are further apart, so it is reasonable to suppose that it is less than 0.25 eV. We are not aware of any calculations of the CTE binding energy for a BHJ cell.

The ionization of the electron-hole pair by an electric field has been analyzed by three related models.

Onsager model. The Onsager model has a geminate electron-hole pair formed with a certain separation that depends on the thermalization of the carriers after the absorption of a photon.[25] The model then considers the relative probability that the pair diffuses apart with help from the field or diffuses together and recombine. The Onsager model does not include a bound exciton state of moderate energy. While the Onsager model seems to apply in certain materials (for example, selenium),[26] many instances of photogeneration in organics do not give reasonable results, in particular, the range of zero-field generation rates that are observed.[27]

Braun model. Braun recognized that the electron-hole pair has a bound exciton state that can be reasonably shallow and should have a relatively low recombination rate ($\sim 10^8$ s^{-1}) so that a significant zero-field ionization rate is possible.[27] Wojcik and Tachiya[28] have recently refined the theory. For a bound state of energy E_B, the probability of ionization is

$$K_I = \frac{\omega_0 \exp(-E_B/kT) f(F)}{K_R + \omega_0 \exp(-E_B/kT) f(F)}, \tag{5}$$

where ω_0 is the attempt to escape prefactor, F is the electric field, and $f(F)$ is the field dependence of the ionization rate, and is a function of $e^3F/8\pi\varepsilon\varepsilon_0 k^2T^2$, where $\varepsilon\varepsilon_0$ is the dielectric constant.

Braun applied a diffusion model to show that the ionization rate in an applied field scales with the zero-field rate such that an exciton with low binding energy ionizes at $\sim 10^5$ V/cm while those with higher binding energy require a substantially higher fields. Braun calculated the value of ω_0 to be $\sim 10^{15}$ s^{-1}. However, in a similar context Mott pointed out that ω_0 cannot be larger than a phonon frequency which is $\sim 10^{13}$ s^{-1}.[29] We use this smaller value in the analysis given below.

Poole-Frenkel model. The Poole-Frenkel effect is the classic model for the field ionization of a bound electron-hole pair and is based on the energy lowering of the potential well by the applied field. The model relies of the energy required to overcome a barrier rather than diffusion over the barrier but otherwise makes the same assumptions as Braun. In the Poole-Frenkel analysis, the energy barrier is lowered by $\Delta E = (\beta F)^{1/2}$, and hence the ionization rate increased by $\exp[(\beta F)^{1/2}/kT]$. Here $\beta = e^3/\pi\varepsilon\varepsilon_0$ and the exponent is the same quantity as in the Braun model apart from the numerical constant. Since the barrier is lowered in the direction of the field, raised in the opposite direction and intermediate in between, various models have tried to take this into account. One formula for the rate increase that accounts for the directional average is[30]

$$f(F) = \left[\frac{(\beta F)^{1/2}}{kT}\right]^{-1} \sinh\left[\frac{(\beta F)^{1/2}}{kT}\right]. \tag{6}$$

A calculation of the field dependence of the exciton ionization based on Eq. (6) agrees well with the Braun results and Fig. 9 shows a fit to the photocurrent current based on the Poole-Frenkel barrier lowering of an exciton with different binding energies. If the energy is large, a high field is required and when the binding energy is small, the ionization is already large and so there is very little field enhancement. The model agrees with the estimate that when the binding energy is 0.25 eV or less, ionization occurs with high probability. The model gives a reasonable fit to the data when the binding energy is ~0.23 eV, as others have reported.[7]

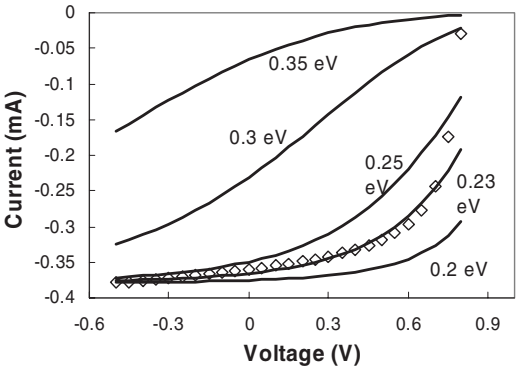

FIG. 9. Photocurrent data (points) and predictions (lines) for the field dependence of the photocurrent, based on a Poole Frenkel model for the electric field ionization of the CTE, assuming different exciton binding energies as indicated.

D. Nongeminate exciton recombination

Even if the charge-transfer exciton ionizes with high probability, a nongeminate CTE may form by the mutual capture of an electron and hole at the interface, and may contribute to the recombination. The exciton forms a quasi-equilibrium with the electron and hole, according to the reaction

$$\text{CTE} \leftrightarrow e + h(\Delta E).$$

The relative balance between the two sides of the reaction is determined by the relative energies. E_{GI}-E_B is the energy of the exciton and E_{GI}-E_{QFE}-E_{QFH} is the energy of the electron-hole pair, where E_{GI} is the band gap at the interface, and $E_{QFE,QFH}$ are quasi-Fermi energies. The difference is

$$\Delta E = E_{QFE} + E_{QFH} - E_B = 0.3 + 0.3 - 0.23 = 0.37 \text{ eV}. \tag{7}$$

The earlier estimates of the QFEs show that each is about 0.3 eV, so the separated pair is the low-energy state by $\Delta E \sim 0.37$ eV even at 1 sun illumination. This energy reduces the effective recombination rate through the CTE by $\exp(-\Delta E/kT) \sim 10^{-6}$. Hence recombination through the charge-transfer exciton has low probability with an estimated recombination time of $10^{-8}/10^{-6}=10^{-2}$ s, compared to the hole lifetime of $10^{-7}-10^{-6}$ s.

In addition, the nongeminate recombination has bimolecular kinetics while the observed kinetics are monomolecular. This mechanism might gain in importance at higher levels of illumination where the QFLs are smaller and would also be more significant in lower mobility materials where the hole concentration is higher.

E. Recombination at interface defects

Under the circumstance that the CTE is sufficiently shallow for a high probability of ionization at zero electric field, recombination of the free carriers can occur at defect or impurity states in the band gap which are at or near the interface. Such states need to have the property that they act as traps for both electrons and holes. Recombination then occurs by sequential capture of an electron and a hole in an order which is determined by the specific electronic characteristics of the trap. The overall recombination rate is determined by the slower of the two trapping events. Trapping of one carrier without recombination, is not sufficient to account for the $P_C(V)$ characteristics, as either the traps will fill completely, effectively removing them from consideration, or the trapped carriers will be excited back to the band edge and will be collected at the contact. A buildup of trapped carriers has been reported in BHJ cells from transient photoconductivity measurements.[31]

Carrier trapping is usually described by the Hecht expression,[32]

$$\frac{Q}{Q_0} = \frac{\mu\tau(V_S - V)}{dd'}\left\{1 - \exp\left[-\frac{dd'}{\mu\tau(V_S - V)}\right]\right\}, \quad F = \frac{V_S - V}{d}, \tag{8}$$

where F is the collection field, d is the sample thickness, and d' is the collection length so that Eq. (8) allows for charges generated in the middle of the cell. Q/Q_0 is the fraction of the generated charge that is collected by the electrodes rather than trapped, and is equal to the current as a fraction of the reverse saturation current, and hence equal to $P_C(V)$. The charge collection involves holes in the polymer and electrons in the PCBM, so the parameter $\mu\tau/dd'$, which determines the shape of the voltage dependence, is a property of both materials. The data in Fig. 10 shows that this model gives an excellent fit to the current-voltage data for a range of different illumination intensities covering a factor ~40.

Figure 11 shows that the parameter $\mu\tau/dd'$, extracted from fits to the data, is reasonably independent of light intensity, and has an average room-temperature value of about 6. The independence on light intensity shows that monomolecular recombination kinetics apply, otherwise the value of $\mu\tau/dd'$ would decrease as the light intensity increases. The conclusion of monomolecular kinetics applies for any recombination model since it is based on the observation that $P_C(V)$ does not change shape with light intensity.

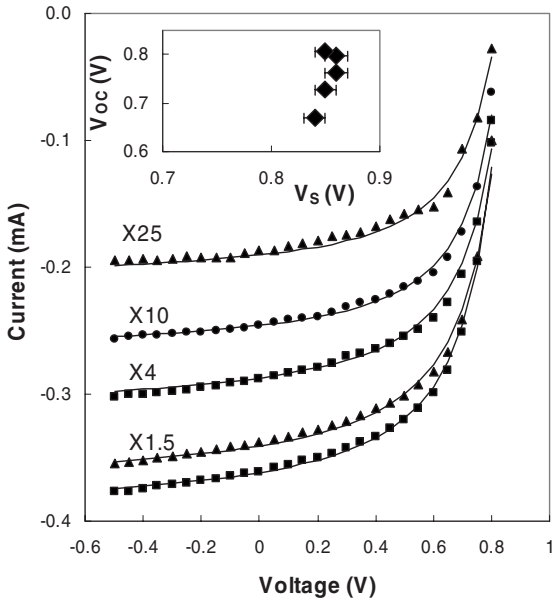

FIG. 10. Photocurrent data with dark current subtracted at different illumination intensities with the data scaled by the factors shown. The solid lines are the fit to Eq. (8) and the fitting parameter $\mu\tau/dd'$ is $6 \pm 10\%$ for all the data. The inset shows that V_S [in Eq. (8)] is constant while the open circuit voltage, V_{OC}, changes significantly with light intensity.

Assuming that the electric field is uniform and the average collection length is half the cell thickness ($d'=d/2$) gives $\mu\tau \sim 3\times10^{-10}$ cm^2/V. The number of recombination centers needed for this mechanism can be estimated as follows, but absent any measured properties or other knowledge of the traps, the estimate is very approximate. For a normal trapping process, with N_R recombination centers per unit volume,[33]

$$\mu\tau = \frac{cel_S}{kT\sigma N_R}, \tag{9}$$

where σ is the capture cross section, l_S is the carrier scattering length, and the constant c depends on the details of the

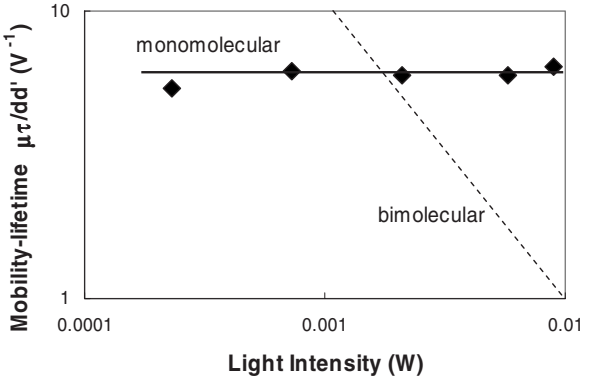

FIG. 11. Mobility-lifetime product ($\mu\tau/dd'$) obtained from the fits to the photocurrent data as a function of light intensity in Fig. 10. The dashed line shows the expected dependence on intensity for a bimolecular recombination mechanism.

transport and trapping mechanism. Capture cross sections vary widely but many are in the range $10^{-15}-10^{-14}$ cm^2. In a study of a disordered semiconductor with diffusing carriers and bulk traps, the value of $\mu\tau N_R$ was found to be in the range 10^7-10^8 cm^{-1} V^{-1}.[27] Assuming that the same trap parameters apply to the BHJ cell, leads to an effective volume trap density of $3\times10^{16}-3\times10^{17}$ cm^{-3}. The equivalent interface state density is $3\times10^{10}-3\times10^{11}$ cm^{-2} since the surface-to-volume ratio of each domain is $\sim10^6$ cm^{-1}. It is reasonable to deduce the interface trap densities in this way (at least to this level of accuracy) because the hole diffusion length, $\sqrt{(D\tau)}\sim20$ nm, is of order the width of the domain. The hole will sample both the surface and the volume of the domain so that it does not substantially affect the recombination rate estimate if the traps are at the interface.

The estimate of $\mu\tau$ is sensitive to the assumption of uniform vertical domains. The presence of disorder in the size and orientation of the domains will increase the domain length and reduce the electric field component in the direction of motion. Both effects will increase the estimated value of $\mu\tau$ but it is difficult to estimate by how much. The value of $\mu\tau$ is an average over the distribution of domains

IV. DISCUSSION

Only the geminate CTE and interface state recombination are viable recombination models, the other two processes being excluded by the monomolecular kinetics and by the rate estimates. Our conclusions apply to the range of illumination intensities studied, which are below 1 sun equivalent values. Bimolecular recombination rates increase with intensity faster than monomolecular rates and therefore may become important at higher illumination intensity. Increased recombination rates reduce the fill factor of the solar cells because of the enhanced recombination rates. The cells we studied have fill factor of 0.59 at 1 sun solar intensity, compared to our measurements of 0.62 at the lower illumination intensity of our measurements. The small difference in fill factor indicates that there can be no more than a minor contribution of bimolecular recombination at solar intensity illumination.

Two aspects of the measurements provide further evidence that the interface state recombination is the dominant mechanism and these are discussed next.

A. Temperature dependence of the photocurrent

Field ionization of the CTE has a specific prediction for the temperature dependence of the $P_C(V)$ characteristics. Figure 12 shows the calculated temperature dependence of the ionization probability obtained from the Braun model with an assumed binding energy of ~0.23 eV. Comparison with Fig. 9 confirms the similarity of the Poole Frenkel and Braun models. However, the model in Fig. 12 is not a good fit to the data in Fig. 4, the difference being both qualitative and quantitative. The field ionization model predicts a more rapid decrease in the current near V_S as the temperature is reduced to ~220 K than is seen in the data. Also the shape of the Braun model is different from that of the data. The

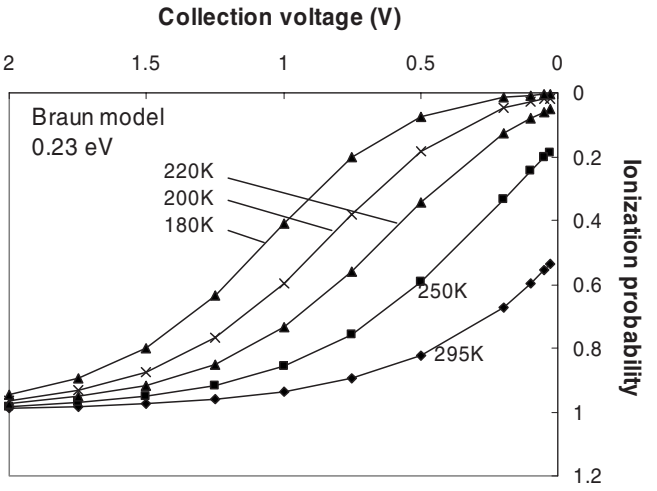

FIG. 12. Calculated temperature dependence of the CTE ionization mechanism based on the Braun model [Eq. (5)]. The collection voltage is V_S-V. The axes are arranged to match the data in Fig. 4.

decrease with temperature is largest at low collection voltage because the carriers need to overcome the full energy barrier of the exciton. At a higher collection voltage, the electric field reduces the energy barrier and the temperature dependence gets correspondingly weaker. The ionization probability curves are shifted to higher voltage at low temperature but this behavior is not seen in the data. We conclude that field ionization of the CTE is inconsistent with the temperature-dependent measurements. Since the field ionization model shows no sign of applying down to 150 K, the binding energy must be substantially smaller than the room temperature estimate of 0.23 eV, and probably not more than 0.15 eV.

On the other hand, Eq. (8) for the charge collection with interface state recombination provides a good fit to the photocurrent data over the whole temperature range, with individual fits shown in Fig. 4. Figure 13 shows the temperature dependence of the parameter $\mu\tau/dd'$, extracted from the fit to Eq. (8), along with data from another sample. The two data sets show the same trend that $\mu\tau/dd'$ increasing roughly proportionally with temperature but with slightly different slopes for the different data sets.

The parameter $\mu\tau$ is proportional to the inverse of the capture cross section [see Eq. (9)], which therefore increases at low temperature. From Eq. (9), the capture cross section has temperature dependence, $\sigma\sim1/\mu\tau T$, and the inset of Fig. 13 shows that the cross section increases by about an order of magnitude at low temperature. The expected temperature dependence of the interface states cross section is not known in the absence of a specific model for the interface states. Since there is no energy barrier to overcome for capture by a deep state, there is no expectation that the cross section will be thermally activated. Note that the temperature dependence of the mobility due to shallow trapping is cancelled out by a corresponding change in the lifetime and so does not affect the $\mu\tau$ product. In crystalline semiconductors, the capture cross section is known to increase with reduced temperature, if there is Coulomb attraction or if the trap has a shallow intermediate state. In amorphous silicon the cap-

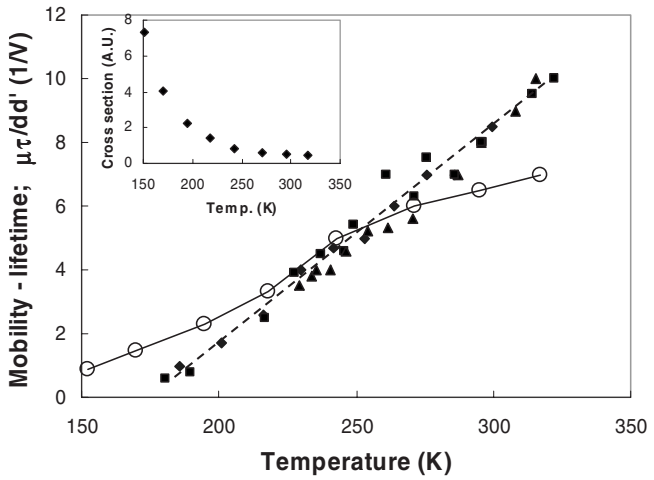

FIG. 13. Values of $\mu\tau/dd'$ as a function of temperature obtained from the fit of photocurrent measurements, such as in Fig. 4, to Eq. (8). Open and closed symbols are for two different samples. The inset shows the temperature dependence of the captured cross section derived from Eq. (9).

ture cross section also increases at lower temperature, an effect that has been attributed to the presence of shallow states close to the recombination center that contribute to the capture process.[33] The observed temperature dependence of $\mu\tau$ is therefore not unusual.

B. Diode dark current characteristics

The diode forward current in the dark also involves electron-hole recombination at the interface. The two main mechanisms used to describe the forward bias diode current for a heterojunction device are such that an ideality factor of $n=1$ corresponds to band-to-band recombination and an ideality factor of 2 arises from the generation-recombination mechanism and requires states near the middle of the interface gap.[34] The BHJ diode may also have recombination at one or other contact for which the ideality factor is unity. There is a high injection mechanism that can give $n=2$ but does not apply at the low voltages used here.

The measured value of $n\sim 1.65$ is consistent with the generation-recombination mechanism, and the reduced value of n arises because either the dominant recombination centers are not at the center of the gap, or the electron-phonon coupling makes the sum of the two transition energies larger than the interface band gap. Hence the diode characteristics indicate that recombination through states in the interface gap may be the dominant mechanism, consistent with the proposed trap mechanism for recombination under illumination.

The band-to-band and gap state recombination mechanisms compete with each other and the dominant mechanism depends on the band-gap energy and the density of interface states. The generation-recombination mechanism is so called because the recombination rates and the thermal generation rates are related by detailed balance. It is easier to consider the relative generation rates. The rate of excitation of a hole across the interface band gap is proportional to $N_{VI}kT\exp(-E_{GI}/kT)$, where N_{VI} is the density of interface states at the valence-band edge. Excitation through a charge-transfer exciton has approximately the same rate because we must include both the excitation to the exciton state and the additional excitation to create free carriers. The equivalent rate of excitation through midgap interface states is $\sim N_R kT\exp(-E_{GI}/2kT)$. Therefore the midgap states dominate when

$$N_R kT\exp(-E_{GI}/2kT) > N_{VI}kT\exp(-E_{GI}/kT),$$

from which

$$N_R > N_V\exp(-E_{GI}/2kT), \quad N_R > 4\times 10^{-11}N_{VI},$$

$$\text{when } E_{GI}=1.2 \text{ eV}. \tag{10}$$

This estimate indicates that N_R would have to be less than $\sim 10^4$ cm^{-2} eV^{-1} for the band-to-band transition to dominate the diode characteristics. This is a very small interface state density even for a single-crystal semiconductor, so it seems highly plausible that there are more interface states than this at the polymer blend heterojunction interface. Hence, the diode forward current strongly indicates the generation-recombination mechanism, from which it follows that interface states provide the dominant mechanism for the recombination of electrons and holes in dark forward bias. If this is true for the dark forward bias, it should also be true of the photocurrent, since the illumination simply injects more carriers into the diode.

We can estimate the number of interface states from the magnitude of the forward current, although very approximately. The reverse bias saturation current, J_0, for the generation-recombination mechanism, is the rate of charge excitation through the interface gap states. The current is the product of the density of states and the excitation rate,

$$J_0 = AeN_R kT\omega_0\exp(-E/kT). \tag{11}$$

N_R is density of states per unit area of the interface and per electron volt and it is assumed that there is a distribution of states and the maximum excitation rate comes from a band of states of width $\sim kT$. E is relevant excitation energy, for which the best estimate is E_{GI}/n, since this value will give the observed ideality factor. A is the area factor for the BHJ structure, i.e., the ratio of the effective internal and the external surface areas. There are two components to A; one is the approximately $10\times$ larger internal surface area of the domains compared to the external surface; the second is that the diode current predominately flows through the center of the domain, where the electron and hole concentrations are similar. We assume that these terms roughly cancel and set $A=1$.

From the measured forward characteristics in Fig. 6, we estimate an interface state density of 10^8–$10^{11}/\text{cm}^2$. The calculation is very sensitive to the magnitude of the interface band gap, which is not known precisely, and to the extrapolated value of J_0. Given all the uncertainties, the estimates of the interface state density is in reasonable order of magnitude agreement with the state density estimated from the capture cross section.

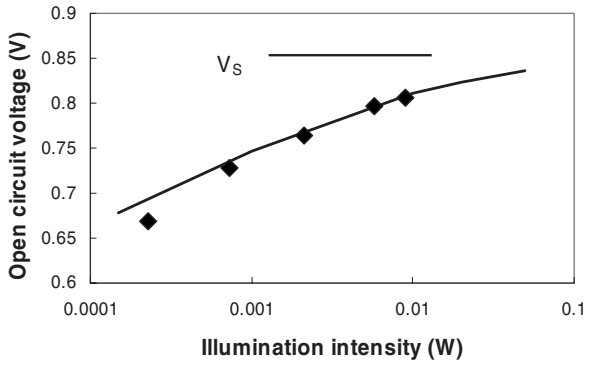

FIG. 14. The measured illumination intensity dependence of V_{OC} (points) compared to a fit (line) to Eq. (14). V_S is indicated for comparison.

C. Relation between V_{OC} and V_S

V_S is the voltage at which the photocurrent changes sign, which is when the internal field changes direction. V_S therefore defines the flat band voltage, V_F, but could be modified by a voltage drop at the contacts due to the series resistance,

$$V_S = V_F + JR_S. \tag{12}$$

The observation that V_S is independent of light intensity (Fig. 10) and therefore independent of current, means that JR_S must be negligible, at least for that range of illumination intensities.

By the definition in Eq. (1), $J_G(V_{OC})=0$, so that,

$$J_{DARK}(V_{OC}) = eP_C(V_{OC})G_{PH}. \tag{13}$$

Setting $V_{OC}=V_S-\delta$, then for the exponential region of the diode dark current characteristics, from Eqs. (2) and (8),

$$J_0 \exp\left(\frac{eV_S}{nkT}\right)\exp\left(-\frac{\delta}{nkT}\right) = eG_{PH}\frac{\mu\tau\delta}{dd'}[1-\exp(-dd'/\mu\tau\delta]. \tag{14}$$

For a reasonably small δ (<0.2 V), such that the exponential on the right side of Eq. (14) is negligible,

$$\delta = nkT\left\{\ln\left[\frac{J_{DARK}(V_S)}{\phi\delta}\right] - \ln(eG_{PH})\right\}, \tag{15}$$

where $\phi=\mu\tau/dd'$. V_{OC} is therefore expected to vary with light intensity approximately as $nkT\ln(eG_{PH})$ when $eG_{PH} \ll J_{DARK}(V_S)$ and saturate at $V_{OC}\sim V_S$ at higher illumination. The intensity dependence data is consistent with this model, as shown in Fig. 14. The fit in Fig. 14 has no adjustable parameters, since it only involves measured quantities, V_S, the dark current, the light intensity and the charge collection parameter. V_{OC} may increase above V_S at higher intensities due to the series resistance at the larger currents, since we know from the dark forward bias characteristics that the series resistance becomes significant in the diode current at about 0.9 V, which is just above V_S in these samples.

The dark forward current is determined by the carrier concentrations at the interface and hence by the Fermi energies on either side, which line up with the contact work function, in the absence of a voltage drop due to the contact resistance. In the same way, the photocurrent across the interface is determined by the photoexcited carrier density and hence by the quasi-Fermi energies. At 1 sun illumination, and near V_{OC}, the dark and photoexcited carrier concentrations are similar, so that the dark Fermi energy and the QFEs must be at similar energies, giving the relation

$$eV_{OC} \approx E_{GI} - E_{\mathrm{QFE}} - E_{\mathrm{QFH}} \tag{16}$$

In Sec. III A, the QFEs were calculated to be about 0.3 eV from the band edge, so together with $V_{OC}\sim 0.8$ V, suggests that the interface gap is ~ 1.4 eV rather than the 1.2 eV obtained from the cyclic voltammetry data of the highest occupied molecular orbital and lowest unoccupied molecular orbital energy levels of the polymer and PCBM. The inaccuracies of the estimates and the complication that the ideality factor is 1.65 rather than 2, make the estimate uncertain, but 1.2 eV seems too low to be consistent with the cell data. The higher value of E_{GI} corresponds to the upper end of the estimated range of interface state density obtained from the forward current and so is more consistent with the estimate of $\sim 10^{11}/\mathrm{cm}^2$ obtained from the charge collection. A more accurate value of the interface band gap would be very helpful for the analysis of BHJ cells.

D. Spectral response

The measurement in Fig. 5 of the spectral response of the solar cell down to low photon energy was made to see if evidence for a direct optical transition through interface states could be found. The response does extend well below the band gaps of either PCDTBT or PCBM which are about 1.9 eV. Indeed, the spectral response has a measurable onset at ~ 1 eV and could extend lower with a more sensitive measurement. The results strongly suggest that there is optical absorption at the interface band gap that excites a photocurrent. However, we cannot easily differentiate whether the observed spectrum is due to direct excitation of the CTE or to transitions involving interface states, or both. The observed onset at 1 eV is just consistent with an interface energy gap of 1.2 eV and a CTE binding energy of 0.15 eV. However, if the interface gap is as large as 1.4 eV as discussed above, the CTE threshold should be at 1.25 eV, significantly above the observed threshold. In this case the low-energy region could be explained by transitions from interface states.

E. Improving the solar-cell efficiency

The assumption that transitions through interface states are the dominant recombination mechanism allows a prediction of the increase in cell efficiency that might be possible if the density of interface states can be reduced. Figure 15 shows the result of a model calculation. The points are the same data as shown in Fig. 1 for one of the cells and the solid line though the data is the best fit based on the charge collection model. The other solid lines correspond to increasing the value of $\mu\tau$ by $2\times$ and $5\times$, as indicated in the figure. There is only about a 10% increase in short circuit current but the fill factor increases significantly, raising the cell effi-

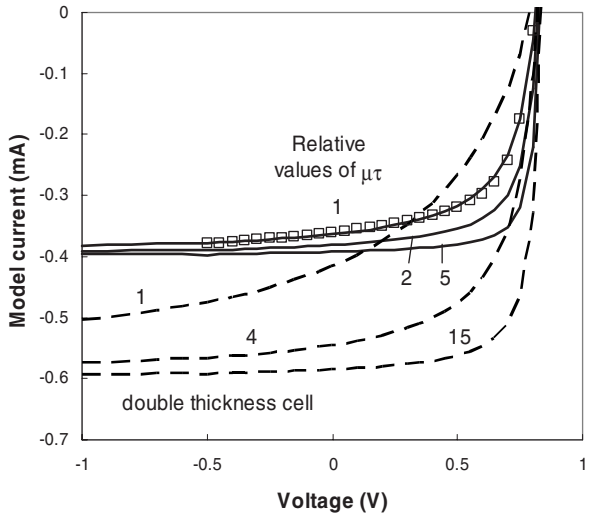

FIG. 15. Calculations of the predicted solar-cell response assuming different values of the mobility-lifetime product. Symbols are data for one of the cells. Solid lines are calculated based on recombination through interface states according to the charge collection model of Eq. (8). The solid lines show the change when $\mu\tau$ is increased by the factors shown. The dashed lines assume the cell thickness is doubled and the saturation current is increased by 50% due to the increased absorption.

ciency, but little more is gained in efficiency by increasing $\mu\tau$ further.

However, when recombination can be suppressed and $\mu\tau$ increased, it is advantageous to increase the cell thickness, because more light is absorbed in the cell and consequently the reverse saturation current increases. The dashed lines in Fig. 15 result from a model in which the cell thickness is doubled to 200 nm but otherwise has the same properties as the thinner cell. The model assumes the saturation current increases by 50%, which seems consistent with the known absorption data. The model calculation with no increase in $\mu\tau$ has a lower efficiency than the thinner cell because the charge collection decreases with thickness [see Eq. (8)]. However, the model calculations with a much larger $\mu\tau$ have both a high short circuit current and high fill factor. The model suggests that an order of magnitude reduction in the interface state density and the corresponding increase in $\mu\tau$, together with a thicker cell, could potentially double the cell efficiency compared to present devices.

V. SUMMARY

The data and analysis described here suggest that recombination at interface states, rather than at charge transfer excitons, is the dominant mechanism that determines the shape of the solar-cell characteristics for the BHJ solar cell. The evidence is the measured recombination kinetics, the form of the temperature dependence which is inconsistent with the CTE mechanism, the dark diode characteristics, and modeling studies which together provide a consistent interpretation with the interface state mechanism. If the mechanism is confirmed, then obviously studies should try to reduce the state density, as this should increase the solar-cell efficiency.

Absent the equivalent data and analysis, we do not know if the same mechanism applies to other BHJ materials, but it is reasonable to suppose that the mechanism is general. We know that the shape of $I_{PC}(V)$ is similar in high efficiency P3HT/PCBM, and the dark diode characteristics are also similar. Measurement of the temperature dependence of $I_{PC}(V)$ should be able to differentiate the mechanisms. There are many cells for which the cell efficiency is low and $I_{PC}(V)$ does not reach saturation until a high collection bias is applied. Such devices might have a particularly high interface state density or possibly might have a CTE that does not ionize easily.

ACKNOWLEDGMENTS

The authors are grateful to A. Heeger for enabling the collaboration to study PCDTBT solar cells, to S. H. Park for help with device fabrication, and to C. Paulson for help with the experimental apparatus. The research at UCSB was funded by the Department of Energy (BSE-DOE ER46535) and the Air Force Office of Scientific Research (AFOSR under Grant No. FA9550-08-1-0248), Charles Lee, Program Officer.

*street@parc.com

[1] J. Y. Kim, K. Lee, N. E. Coates, D. Moses, T. Q. Nguyen, M. Dante, and A. J. Heeger, Science **317**, 222 (2007).
[2] N. S. Sariciftci, L. Smilowitz, A. J. Heeger, and F. Wulf, Science **258**, 1474 (1992).
[3] S. H. Park, A. Roy, S. Beaupre, S. Cho, N. Coates, J. S. Moon, D. Moses, M. Leclerc, K. Lee, and A. J. Heeger, Nat. Photonics **3**, 297 (2009).
[4] B. M. Kayes and H. A. Atwater, J. Appl. Phys. **97**, 114302 (2005).
[5] A. Liu, S. Zhao, S.-B. Rim, J. Wu, M. Könemann, P. Erk, and P. Peumans, Adv. Mater. **20**, 1065 (2008).
[6] L. J. A. Koster, V. D. Mihailetchi, and P. W. M. Blom, Appl. Phys. Lett. **88**, 093511 (2006).
[7] T. Kirchartz, B. E. Pieters, K. Taretto, and U. Rau, J. Appl. Phys. **104**, 094513 (2008).
[8] M. M. Mandoc, L. J. A. Koster, and P. W. M. Blom, Appl. Phys. Lett. **90**, 133504 (2007).
[9] P. Peumans and S. R. Forrest, Chem. Phys. Lett. **398**, 27 (2004).
[10] L. J. A. Koster, V. D. Mihailetchi, and P. W. M. Blom, Appl. Phys. Lett. **88**, 052104 (2006).
[11] P. Kumar, S. C. Jain, V. Kumar, S. Chand, and R. P. Tandon, J. Appl. Phys. **105**, 104507 (2009).
[12] By the usual definition, the solar-cell current is negative and the bias voltage is positive in forward bias. As a result the photoconductivity is a negative quantity.
[13] Poly[N-9′-hepta-decanyl-2,7-carbazole-alt-5,5-(4′,7′-di-2-thienyl-2′,1′,3′-benzothiadiazole)].

[14] N. Blouin, A. Michaud, and M. Leclerc, Adv. Mater. **19**, 2295 (2007).
[15] S. Wakim, S. Beaupre, N. Blouin, B.-R. Aich, S. Rodman, R. Gaudiana, Y. Tao, and M. Leclerc, J. Mater. Chem. **19**, 5351 (2009).
[16] Z. E. Ooi, R. Jin, J. Huang, Y. F. Loo, A. Sellinger, and J. C. deMello, J. Mater. Chem. **18**, 1644 (2008).
[17] D. Veldman, O. Ipek, S. C. J. Meskers, J. Sweelssen, M. M. Koetse, S. C. Veenstra, J. M. Kroon, S. S. van Bavel, J. Loos, and R. A. J. Janssen, J. Am. Chem. Soc. **130**, 7721 (2008).
[18] M. Hallermann, S. Haneder, and E. Da Como, Appl. Phys. Lett. **93**, 053307 (2008).
[19] R. Sokel and R. C. Hughes, J. Appl. Phys. **53**, 7414 (1982).
[20] S. Oosterhout, M. M. Wienk, S. S. Van bavel, R. Thiedmann, L. J. A. Koster, J. Gilot, J. Loos, V. Schmidt, and R. A. J. Janssen, Nature Mater. **8**, 818 (2009).
[21] R. A. Street, J. E. Northrup, and A. Salleo, Phys. Rev. B **71**, 165202 (2005).
[22] C. J. Brabec, G. Zerza, G. Cerullo, S. De Silvestri, S. Luzzati, J. C. Hummelen, and S. Sariciftci, Chem. Phys. Lett. **340**, 232 (2001).
[23] N. Tessler and N. Rappaport, Appl. Phys. Lett. **89**, 013504 (2006).
[24] R. A. Street, Appl. Phys. Lett. **93**, 133308 (2008).
[25] L. Onsager, Phys. Rev. **54**, 554 (1938).
[26] J. C. Knights and E. A. Davis, J. Phys. Chem. Solids **35**, 543 (1974).
[27] C. L. Braun, J. Chem. Phys. **80**, 4157 (1984).
[28] M. Wojcik and M. Tachiya, J. Chem. Phys. **130**, 104107 (2009).
[29] N. F. Mott and E. A. Davis, *Electronic Processes in Non-crystalline Materials* (Oxford University Press, New York, 1979).
[30] Ref. 29, p. 97.
[31] I. Hwang, C. R. Mcneill, and N. Greenham, J. Appl. Phys. **106**, 094506 (2009).
[32] K. Hecht, Z. Phys. **77**, 235 (1932); see also R. A. Street, *Hydrogenated Amorphous Silicon* (Cambridge University Press, Cambridge, England, 1991), p. 312.
[33] R. A. Street, Philos. Mag. B **49**, L15 (1984).
[34] http://ecee.colorado.edu/~bart/book/book/chapter4/ch4_4.htm